INTERNATIONAL JOURNAL FOR NUMERICAL METHODS IN FLUIDS, VOL. 12, 1–15 (1991)

INTERNAL THREE-DIMENSIONAL VISCOUS FLOW SOLUTIONS USING THE VORTICITY–POTENTIAL METHOD

HERONG YANG AND RICARDO CAMARERO

Department of Applied Mathematics, Ecole Polytechnique de Montréal, PO Box 6079, Stn A, Montréal, Canada H3C 3A7

SUMMARY

A numerical solution procedure for internal three-dimensional viscous flow is proposed in this paper. The formulation is based on the non-primitive variables, the vorticity and potentials, on a curvilinear grid. A new upwind difference scheme is introduced to overcome the convective instabilities arising in the central difference scheme for the vorticity transport equations, while keeping false diffusion to a minimum level. Developing flows in both straight and curved square ducts are simulated to validate the procedure. The results are compared with both experimental measurements and analytical solutions.

KEY WORDS 3D Viscous flow Vorticity–potential Body-fitted grid Rotated upwind

1. INTRODUCTION

A large number of numerical methods have been developed over the years to simulate laminar internal flows. Most of them are based on the primitive variable equations.[1–8] The earliest[1–3] methods were restricted to the parabolized Navier–Stokes equations. Several modifications[4–6] were subsequently developed for partially parabolized flows in which the viscous influence in the upstream direction is only transmitted by the pressure. Neither parabolized nor partially parabolized approaches are suitable for obtaining solutions to flows in which flow separation is present in the primary flow direction. To overcome such restrictions, several methods[7,8] have also been developed for the solution of the full Navier–Stokes equations. These methods can be very expensive compared with the previous methods but have demonstrated the capability to predict more complex three-dimensional phenomena.

Another class of methods[9–12] based on the vorticity–potential formulation can be regarded as the extension to three dimensions of the well-known 2D vorticity–streamfunction formulation. The main advantages of these methods are that the pressure is eliminated in the governing equation system and that the continuity equation is satisfied by a potential component of the velocity. Using the vorticity–potential method, Mallinson and de Vahl Davis[9] have simulated the natural convection flows in a box. In their studies the potential component of the velocity reduces to zero because there is no flow through the boundaries. Aregbesola and Burley[10] have reported numerical solutions of flows in a duct with one cavity formed on one wall. They computed the potential component of the velocity from the scalar potential function governed by a Laplacian equation. To simplify the calculation of the scalar potential, Wong and Reizes[11] have set the potential component of the velocity to be the streamwise mean velocity. However, this assumption

0271–2091/91/010001–15$07.50

Received 26 July 1988
Revised 9 January 1990

is restricted to straight duct geometries. Recently, Yang and Camarero[12] have proposed a general method for the scalar potential calculation for flows in arbitrary ducts which removes most of the restrictions of previous works.

One problem remaining in the study of Yang and Camarero[12] is the convection instability arising in the central difference scheme for the vorticity transport equations at high Reynolds numbers. In the present paper a stable and accurate difference scheme is proposed to overcome the instability problem. Based on this scheme a computational procedure for general internal viscous flows is presented. Numerical studies of developing flows in both straight and curved square ducts are performed to validate the present procedure.

2. GOVERNING EQUATIONS

The system of equations governing a viscous, incompressible, steady state flow is

$$\nabla' \cdot V' = 0, \tag{1}$$

$$(V' \cdot \nabla')V' = -\nabla' p' + \nu \nabla'^2 V', \tag{2}$$

where V' and p' are the dimensional velocity and pressure respectively and ν is the kinematic viscosity. For the duct flow it is convenient to use the streamwise mean velocity v_i at the inlet and the hydraulic diameter D_h at the inlet as the normalization parameters. The governing equations (1) and (2) can then be non-dimensionalized as

$$\nabla \cdot V = 0, \tag{3}$$

$$(V \cdot \nabla)V = -\nabla p + (1/Re)\nabla^2 V, \tag{4}$$

where

$$\nabla = \nabla' D_h, \qquad V = V'/v_i, \qquad p = p'/v_i^2, \qquad Re = D_h v_i / \nu. \tag{5}$$

The vorticity–potential method is based on the decomposition of the velocity vector into potential and rotational components,

$$V = -\nabla \phi + \nabla \times A, \tag{6}$$

where ϕ and A are the scalar and vector potentials. The existence of the scalar and vector potentials of a given velocity field has been proved by Hirasaki and Hellums.[13] In addition, the vector potential A can be required to satisfy the solenoidal condition

$$\nabla \cdot A = 0 \tag{7}$$

to simplify the application.

Using the scalar and vector potentials, the governing equations (3) and (4) can be transformed into

$$\nabla^2 \phi = 0 \tag{8}$$

$$(V \cdot \nabla)W - (W \cdot \nabla)V = (1/Re)\nabla^2 W, \tag{9}$$

$$\nabla^2 A = -W, \tag{10}$$

where W is the vorticity defined as

$$W = \nabla \times V. \tag{11}$$

Obviously, this set of governing equations has two main advantages compared with that in terms of primitive variables. The continuity equation is satisfied by the scalar potential

independently from other variables, and the pressure, which has no explicit evaluation equation, is eliminated from the system.

In order to facilitate the treatment of the boundary conditions for a general curved duct, the Cartesian co-ordinate system is transformed into a body-fitted curvilinear co-ordinate system. Details can be found in Reference 14.

3. BOUNDARY CONDITIONS

Unlike the primitive variables, the use of the derived variables causes some difficulties in the determination of the boundary conditions. Yang and Camarero[12] have reviewed this problem extensively and have introduced the following set of boundary conditions for the application of duct flows.

Boundary conditions on ϕ:

$$\begin{aligned} &\partial\phi/\partial n = 0 && \text{on the wall,} \\ &\partial\phi/\partial n = -v_i && \text{at the inlet,} \\ &\partial\phi/\partial n = -v_o && \text{at the outlet,} \end{aligned} \tag{12}$$

where v_o is the mean velocity at the outlet.

Boundary conditions on A:

$$\begin{aligned} A_t = \partial A_n/\partial n = 0 \quad & \text{on the wall,} \\ A_t = (\nabla_s \times B)_t, \quad \partial A_n/\partial n = 0 \quad & \text{at the inlet,} \\ \partial^2 A/\partial n^2 = 0 \quad & \text{at the outlet,} \end{aligned} \tag{13}$$

where ∇_s is the surface gradient operator and B is a vector function defined on the inlet section only. The vector B can be computed as

$$B_t = 0, \qquad \nabla_s \times (\nabla_s \times B_n) = V_n - v_i. \tag{14}$$

Boundary conditions on W:

$$\begin{aligned} &W = \nabla \times V && \text{on the wall,} \\ &\partial^2 W/\partial n^2 = 0 && \text{at the outlet.} \end{aligned} \tag{15}$$

It should be noticed that the evaluation of the vorticity at the inlet depends on the type of incoming flow. For example, if the incoming flow is uniform, the vorticity at the inlet can be set to zero. If the incoming flow is fully developed in a straight duct, the vorticity can be computed as

$$\begin{aligned} W_x &= \partial V_z/\partial y, \\ W_y &= -\partial V_z/\partial x, \\ W_z &= \partial V_y/\partial x - \partial V_x/\partial y, \end{aligned} \tag{16}$$

where x and y represent the co-ordinates in the cross-sectional directions while z represents the streamwise direction.

4. ROTATED UPWIND SCHEME

For convection-dominated flows or high-Reynolds-number flows it is well known that central differences result in instabilities for the momentum and vorticity transport equations. The most frequently used technique to overcome this convection instability is the upwind difference scheme.

This ensures unconditional stability but introduces a significant truncation error, also called false diffusion, in multiple dimensions. To reduce the false diffusion, Raithby[15] has introduced the skew upwind difference scheme, which performs an upwind interpolation in the local streamwise direction for the control volume face values. The skew upwind scheme indeed reduces the false diffusion significantly but still suffers from the instability problem.[14]

In order to reduce the false diffusion and still maintain unconditional stability, the conventional upwind scheme is applied in a locally rotated co-ordinate system. The resulting scheme is called the rotated upwind difference scheme, which can be briefly described as follows. At each grid node a rotated co-ordinate system can be established so that one co-ordinate direction coincides with the streamwise direction as illustrated in Figure 1. The convection terms in the vorticity transport equation (9) are then reduced to a one-dimensional form:

$$(V\cdot\nabla)W=\|V\|\,\partial W/\partial s, \tag{17}$$

where s is the streamwise direction and $\|V\|$ is the magnitude of the velocity vector. The conventional upwind difference scheme can be easily applied to this reduced form and the resulting discretization will be

$$\|V\|\frac{\partial W}{\partial s}=\|V\|\frac{W_{\mathrm{P}}-W_{\mathrm{U}}}{\Delta s}. \tag{18}$$

The subscripts P and U denote the grid node and the intersection of the negative s-co-ordinate line with the original grid surface respectively. The values of W can be interpolated from the nearest nodal values.

It should be pointed out that the proposed scheme is very similar to the skew upwind scheme.[15] Both schemes perform an upwind interpolation in the local streamwise direction to reduce the false diffusion. The essential difference is that the present scheme is based on the finite difference formulation in a local co-ordinate system rather than the control volume formulation. This ensures that the resulting algebraic system has no negative coefficients, therefore resulting in an unconditionally stable scheme. The drawback is that the present scheme is non-conservative. However, this will not cause any problem in the present application since the conservative character of the solution is ensured by the potential formulation.

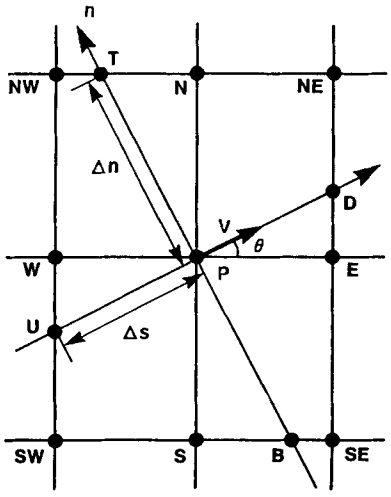

Figure 1. Illustration of rotated co-ordinates

5. COMPUTATIONAL REMARKS

As described above, the convection terms in the vorticity transport equation (9) are discretized by the rotated upwind difference scheme, while the other terms in the governing equations are all discretized by the central difference scheme. Details can be found in Reference 14.

Numerical solutions of the discretized equations are obtained by the block SOR method in which the implicit block contains the nodes in one grid line in a cross-stream direction. The relaxation parameter used is about 1·5 for both the scalar and the vector potential equations, while the vorticity equation is underrelaxed with 0·7.

The overall solution procedure consists of the following steps:

(1) generation of the body-fitted grid
(2) computation of the potential solution
(3) computation of the viscous solution.

The potential solution is computed by a separate computer program, which requires about 10^{-5} s of CPU time per node per iteration on an IBM-4341. In the viscous solution process the vorticity transport equation (9) and the vector potential equation (10) are alternately solved in each cycle. The CPU time required is about $0{\cdot}4 \times 10^{-3}$ s per node per cycle on the same machine. The convergence criterion was set as the maximum difference in velocity between two adjacent cycles being less than 10^{-5}. The total computer time required for the converged solution of a typical problem is about 8 min with a $15 \times 15 \times 31$ grid.

6. NUMERICAL RESULTS AND DISCUSSION

6.1. *Developing flow in straight duct*

Since both experimental measurements[16] and the analytical solution[17] are available for the developing flow in a straight square duct, numerical computations were first carried out for this problem to check the stability and accuracy of the present procedure.

According to the analytical solution of Han,[17] the flow will reach a fully developed condition at an axial distance of $0{\cdot}075\, D_h Re$. So the non-dimensional duct length is set to be $0{\cdot}102Re$ in the present test to ensure that the flow is fully developed within the duct. Figure 2 shows the duct geometry used in the test for $Re = 100$. The grid in the duct is generated algebraically in the following way. First 31 cross-sections are distributed along the duct axis with the following distribution:

$$z_k = \Delta z(k-1)[1{\cdot}0 + 0{\cdot}8(k-1)\Delta z], \tag{19}$$

where z_k is the location of the kth section and Δz is the initial increment of $0{\cdot}001Re$. Then on a given cross-section a uniform grid is used.

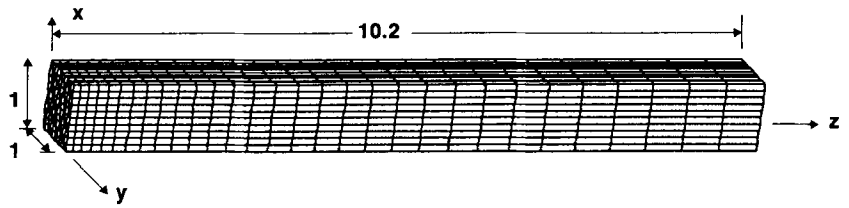

Figure 2. Geometry of straight duct for $Re = 100$

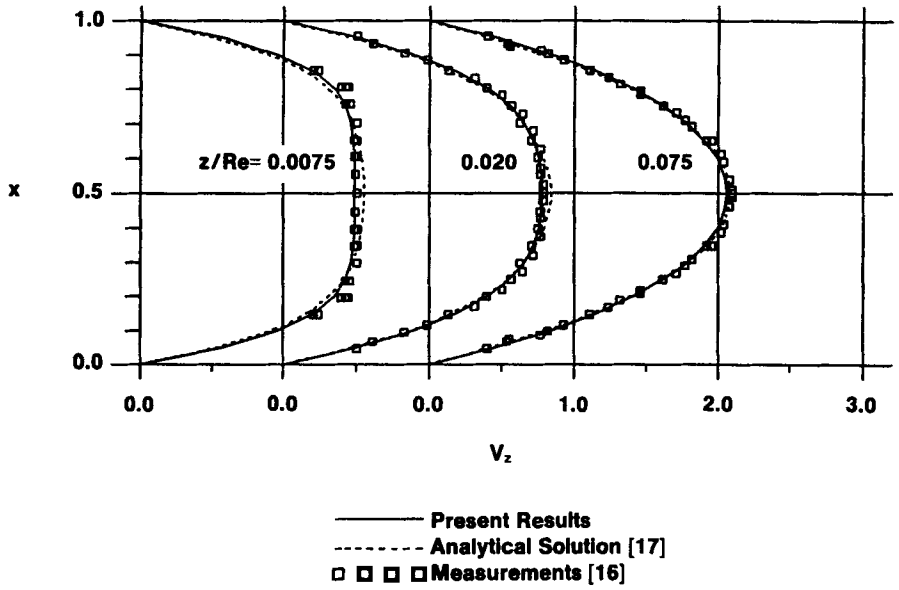

Figure 3. Development of velocity profiles on central plane

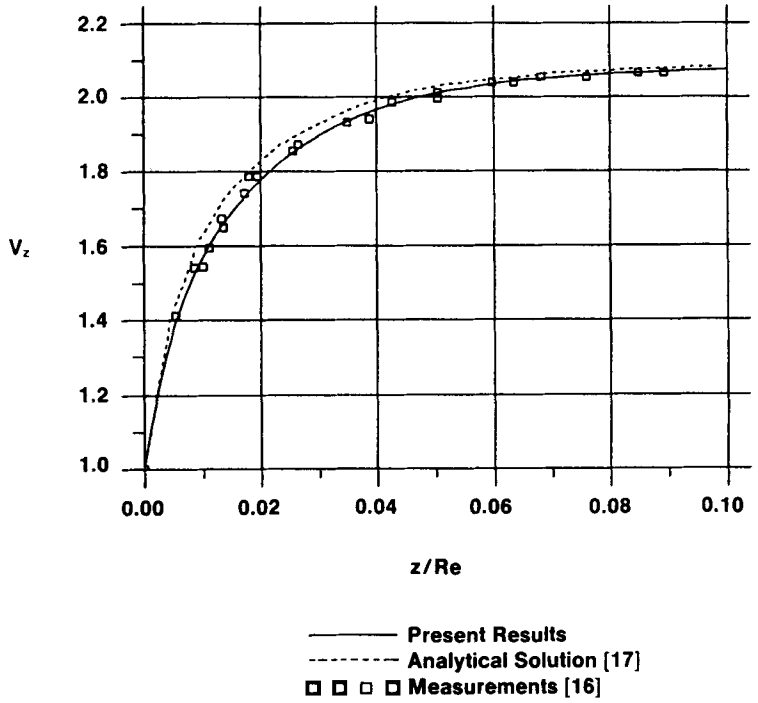

Figure 4. Velocity development along duct centreline

In this simple geometry the potential computation is unnecessary because the exact solution of the scalar potential exists:

$$\phi = -z + c, \tag{20}$$

where c is an arbitrary constant. For the viscous solution, two tests were first performed at $Re = 100$ using 11×11 and 15×15 grids in the cross-sections. The solution processes were quite stable and required about 88 and 160 cycles to obtain the converged solutions respectively. The maximum difference between the two results was about 4%. It was also found that further refinement in the grid would require considerable computer time and storage. Therefore the 15×15 grid was selected in the following numerical computations.

The streamwise velocity profiles on the central plane at the locations $z/Re = 0{\cdot}0075$, $0{\cdot}02$ and $0{\cdot}075$ are presented in Figure 3 for $Re = 100$ together with the experimental measurements[16] and the analytical solution.[17] It can be seen that the computed results agree very well with the measurements, while the analytical solution slightly overpredicts the measurements in the duct centre. Figure 4 shows the development of the centreline velocity. The agreement of the computed results with the experiments is satisfactory. However, differences between the computed results and the analytical solution exist in the region from $z = 0{\cdot}01Re$ to $z = 0{\cdot}06Re$.

In order to see the effects of the Reynolds number, two more viscous computations were carried out at $Re = 400$ and 800. The developments of the centreline velocities for $Re = 100$, 400 and 800 are compared in Figure 5. The streamwise distance is normalized as z/Re in this figure. The differences among the curves are insignificant. This is expected to be correct since the developing

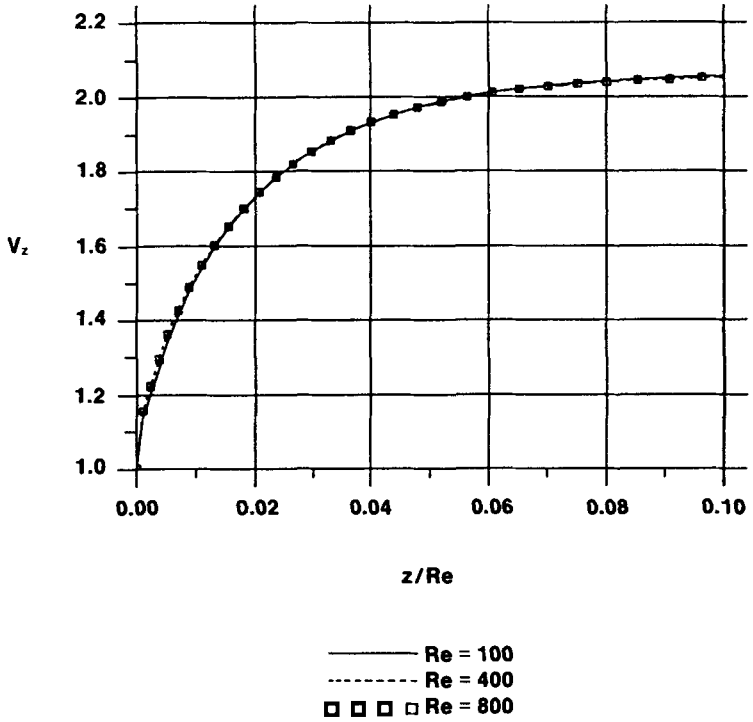

Figure 5. Comparison of centreline velocity for $Re = 100$, 400 and 800

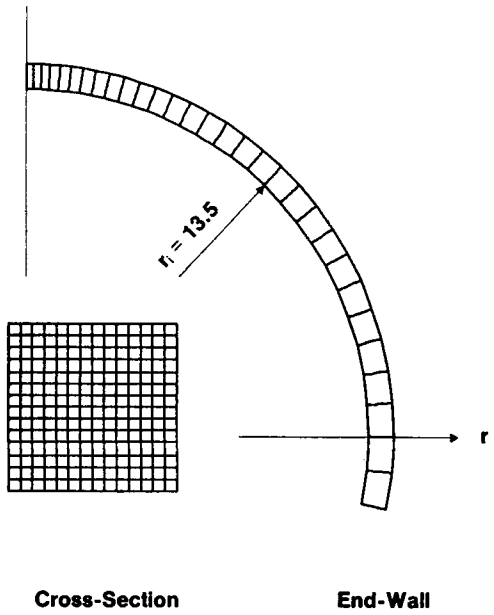

Figure 6. Geometry of curved duct

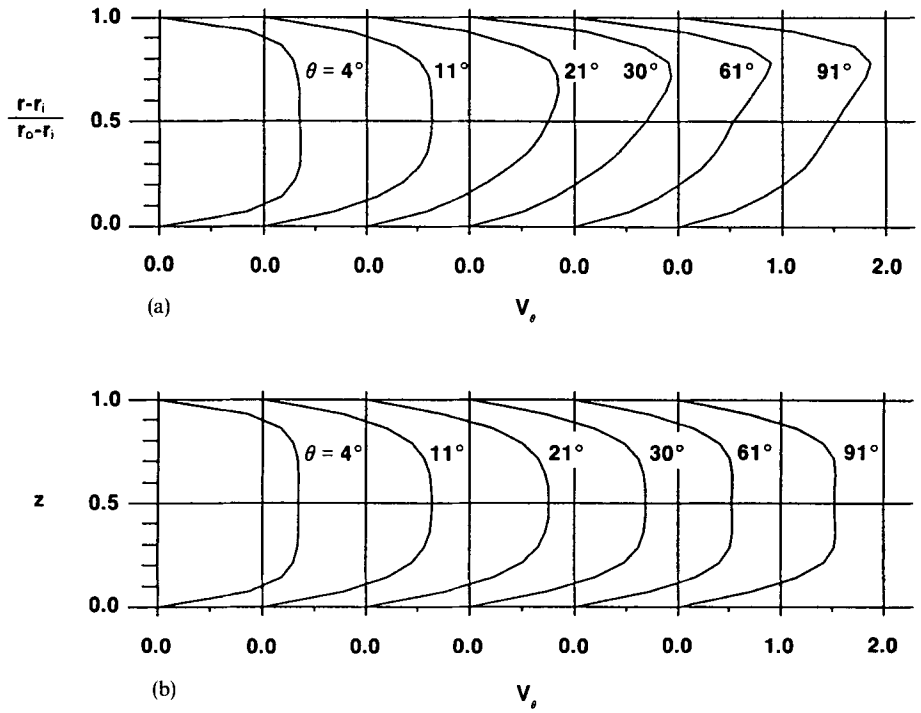

Figure 7. Development of streamwise velocity profiles along (a) r-direction (b) z-direction

flow is characterized only by the dimensionless distance z/Re. Further increase in the Reynolds number would not cause any significant changes in the development characteristics.

6.2. *Developing flow in curved duct*

To test the ability of the present procedure in the prediction of the streamwise curvature, developing flow in a curved duct of square cross-section was simulated. An important feature in curved duct flows is the secondary flow induced in the cross-planes as a result of the centrifugal forces generated by the duct curvature. It is well known that the fully developed curved duct flows are characterized by the Dean number $De = ReD_h/R$, where R is the duct centreline curvature.

The duct geometry is illustrated in Figure 6; the curvature ratio is 14 and the total turning angle is 102°. The grid sections are distributed in a way similar to the straight duct:

$$\theta_k = \Delta\theta(k-1)[1{\cdot}0 + 0{\cdot}8(k-1)\Delta\theta], \tag{21}$$

where θ_k is the location of the kth section and $\Delta\theta$ is the initial increment of $0{\cdot}01Re$. Uniform 15×15 grids are then generated in the sections.

The scalar potential was easily computed. The converged solution was obtained after 330 iterations with a relaxation parameter of 1·3. The viscous solution was then obtained at $Re = 206$, corresponding to $De = 55$. The development of the streamwise velocity profiles is shown in Figure 7. It is seen that the curvature has little influence on the streamwise velocities in the initial

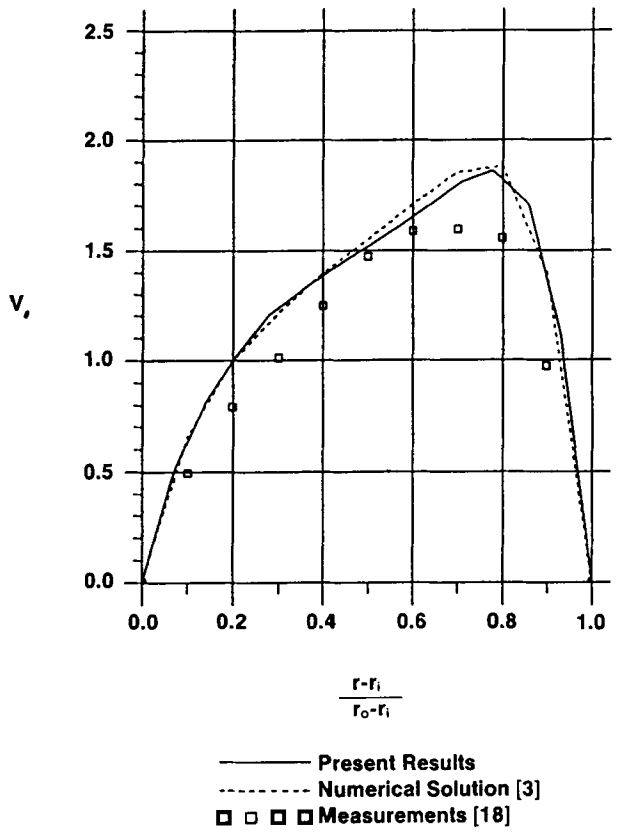

Figure 8(a). Fully developed streamwise velocity profiles along r-direction

portion of the entrance region, and the boundary layer grows symmetrically in both cross-sectional directions. As the flow progresses downstream, the centrifugal forces generated by the curvature become more significant. Consequently, the computed profiles become more asymmetric along the radial direction. The peak value of the velocity shifts towards the outer curved wall of the duct. Along the horizontal direction the profile remains symmetric, as expected. The presence of a hump in this symmetric profile indicates the existence of two streamwise vortices.

In Figure 8 the computed fully developed profiles are compared with available numerical data of Ghia and Sokhey.[3] They used the parabolic flow assumption and a very fine 21 x 21 grid in each cross-section in their calculation. Good agreement can be observed between the two numerical results. Also shown in this figure are the experimental measurements of Mori *et al.*[18] at $De = 51$. The agreement is relatively poor between the numerical results and the measurements; the reason for this has not been fully explained yet.

6.3. Flow in Humphrey's duct

The applicability of the present procedure to curved ducts of strong curvature was tested using the experiment reported by Humphrey *et al.*[8] As shown in Figure 9, the main part of Humphrey's duct is a bend of square cross-section with radius ratio R/D_h of 2·3 and total turning angle of 90°. Two straight extensions are added to the entrance and exit of the bend. The lengths of these extensions are set to $2D_h$ and $5D_h$ in the present test rather than the $30D_h$ and $45D_h$ used in the

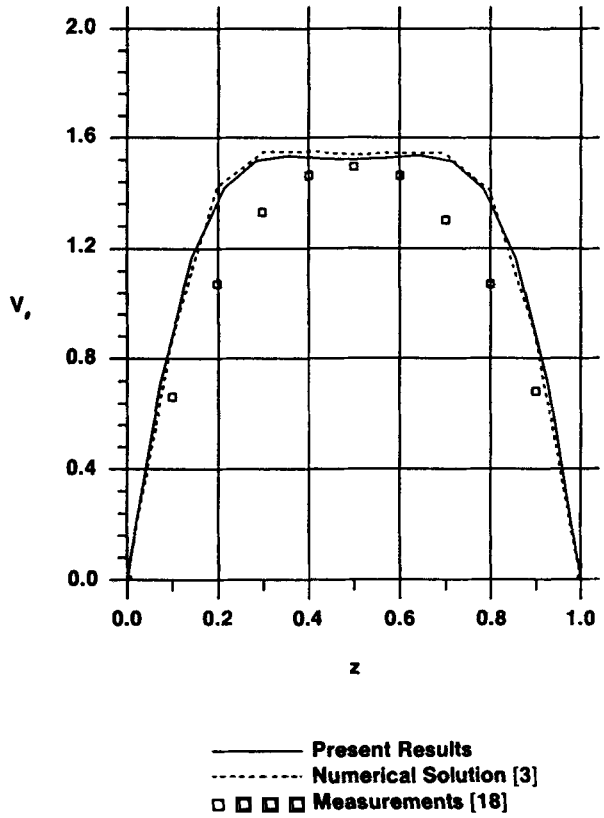

Figure 8(b). Fully developed streamwise velocity profiles along z-direction

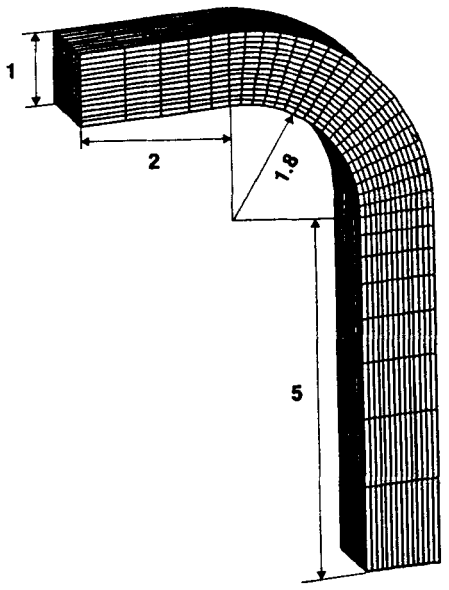

Figure 9. Geometry of Humphrey's duct

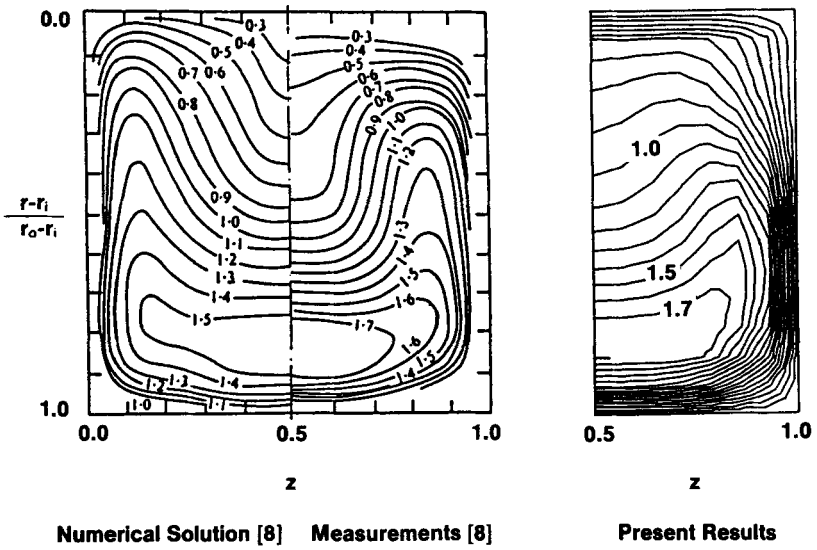

Figure 10(a). Comparison of streamwise velocity contours at $\theta = 60°$

experiment. This is reasonable since it is known from experiment that the evolution of the flow in the upstream part of the duct as well as the downstream extension have little effect on the flow in the bend. The flow Reynolds number used was 790, corresponding to a Dean number of 368. The inlet flow was set to be uniform.

To generate the grid, 19 sections are uniformly distributed along the bend centreline, while in the inlet and outlet extensions, five and eight sections are distributed in such a way that the axial

step is increased by a factor of 1·25 from section to section. Again uniform 15 × 15 grids are used in the cross-sections.

Figure 10 shows the streamwise velocity contours of the computed results on two typical sections of $\theta = 60°$ and 90°. Also shown in this figure are the experimental and computational results obtained by Humphrey *et al.*[8] Their computational results were obtained by the modified parabolic flow method originally developed by Gosman and Pun.[19] In general, the two

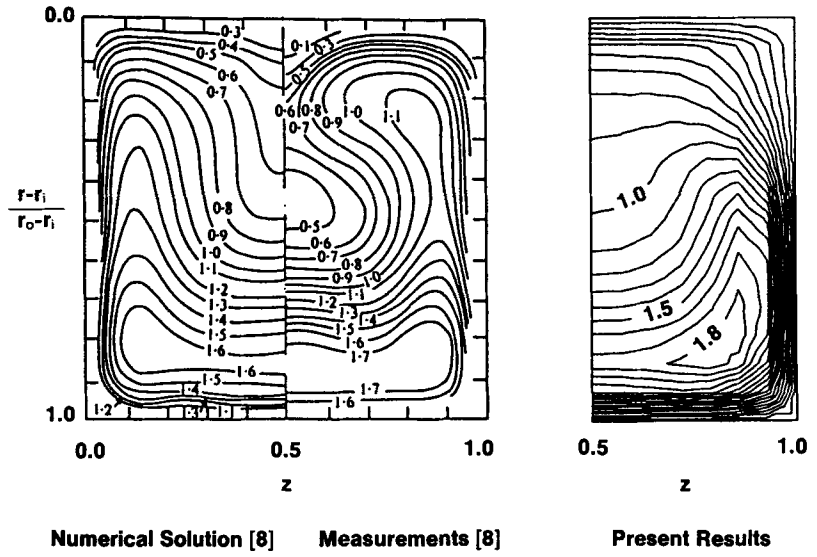

Figure 10(b). Comparison of streamwise velocity contours at $\theta = 90°$

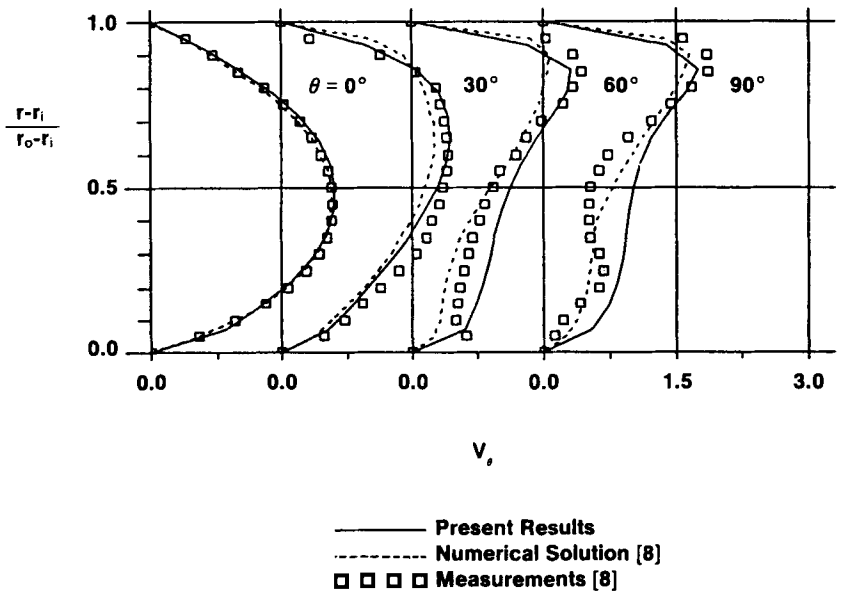

Figure 11. Comparison of streamwise velocity profiles

computational results agree well, although the 15×15 sectional grid used in the present computation is relatively coarse compared with the 10×15 used by Humphrey *et al.* for half the duct. It is seen that the peaks indicated by the measurements are smoothed out by the computations because of the coarse grids, but the trends are well simulated. To provide a close comparison, the streamwise velocity profiles on the central plane are presented in Figure 11. The computational results agree well with the experimental data, except near the end of the bend, where both calculations give smoother variations than the experiment.

A very interesting phenomenon shown in the experiment of Humphrey *et al.* is the existence of two small regions of back flow symmetrically located at the outer wall between 0° and 25° of turning angle and close to the side walls. This phenomenon was subsequently confirmed by their numerical computation and also verified by the present computation. Figure 12(a) shows the

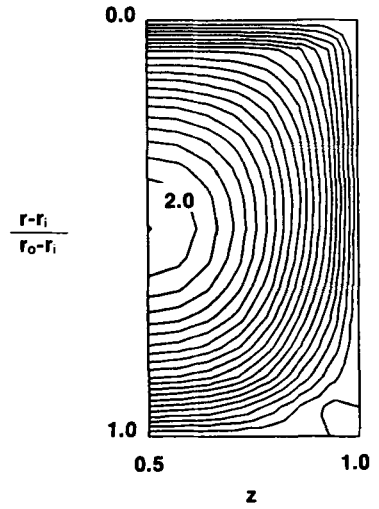

Figure 12(a). Streamwise velocity contours at $\theta = 10°$

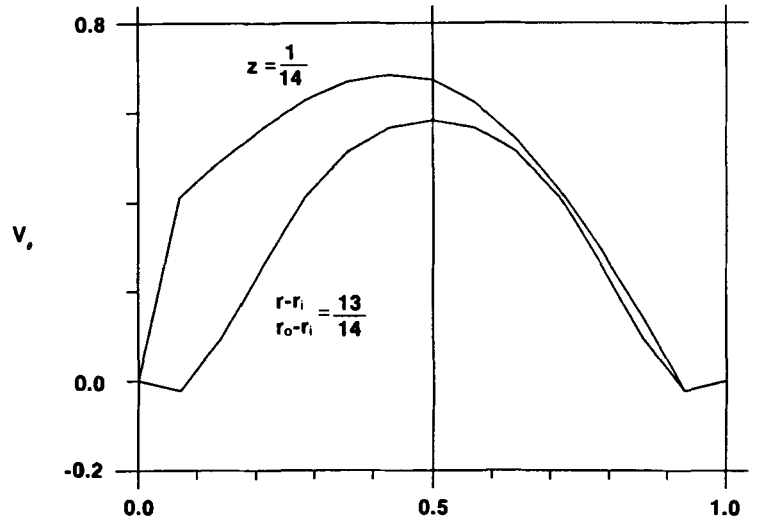

Figure 12(b). Streamwise velocity profiles in back flow region

streamwise velocity contours on the section of $\theta = 10°$. In this figure the zero-velocity curve clearly indicates the size of this back flow region. It is also found that this region does not extend beyond $\theta = 5°$ and 15° in upstream and downstream directions respectively. The streamwise velocity profiles along the grid lines passing through the back flow region are shown in Figure 12(b). The maximum negative velocity is about 0·05 of the sectional mean velocity.

7. CONCLUSIONS

The main purpose of the present work was to develop a computational procedure to simulate 3D internal laminar flows. Numerical solutions have been presented for developing flows in both straight and curved ducts as well as in the laminar flow inside Humphrey's duct. Computed results were compared with the available theoretical and numerical solutions and experimental measurements to validate the stability and accuracy of the present procedure. The essentially fair agreement achieved indicates that the present procedure can be used to obtain laminar duct flow details with an acceptable degree of accuracy. Future works include further tests for cases of blade passages in turbomachinery and passages of varying areas.

APPENDIX: NOMENCLATURE

A	vector potential
D_h	hydraulic diameter at the inlet
p	pressure
Re	Reynolds number
v_i, v_o	mean velocities at inlet and outlet
V	velocity
W	vorticity
v	kinematic viscosity
ϕ	scalar potential

REFERENCES

1. S. V. Patankar and D. B. Spalding, 'A calculation procedure for heat, mass and momentum transfer in three-dimensional parabolic flows', *Int. J. Heat Mass Transfer*, **15**, 1783–1806 (1972).
2. W. R. Briley, 'Numerical method for predicting 3D steady viscous flow in ducts', *J. Comput. Phys.*, **14**, 8 (1974).
3. K. H. Ghia and J. S. Sokhey, 'Laminar incompressible viscous flow in curved ducts of regular cross-section', *J. Fluids Eng.*, 640–649 (1977).
4. U. S. Pratap and D. B. Spalding, 'Fluid flow and heat transfer and three-dimensional duct flows', *Int. J. Heat Mass Transfer*, **19**, 1183–1186 (1976).
5. P. R. Dodge, 'Numerical method for 2D and 3D viscous flows', *AIAA J.*, **15**, 961–965 (1977).
6. J. Moore and J. G. Moore, 'A calculation procedure for three-dimensional, viscous, compressible duct flow, Part I', *J. Fluids Eng.*, **101**, 415–428 (1979).
7. M. Agouzoul, M. Reggio and R. Camarero, 'Simulation of three-dimensional internal turbulent flows', *ASME Winter Annual Meeting*, vol. 69, pp. 19–25, Dec. 1988.
8. J. A. C. Humphrey, A. M. K. Taylor and J. H. Whitelaw, 'Laminal flow in a square duct of strong curvature', *J. Fluid Mech.*, **83**, 509–527 (1977).
9. G. D. Mallinson and G. de Vahl Davis, 'Three-dimensional natural convection in a box, a numerical study', *J. Fluid Mech.*, **83**, 1–31 (1977).
10. Y. A. S. Aregbesola and D. M. Burley, 'The vector and scalar potential method for numerical solution of two- and three-dimensional Navier–Stokes equations', *J. Comput. Phys.*, **24**, 398–415 (1977).
11. A. K. Wong and J. A. Reizes, 'An effective vorticity–vector potential formulation for the numerical solution of three-dimensional duct flow problem', *J. Comput. Phys.*, **55**, 98–114 (1984).
12. H. Yang and R. Camarero, 'An improved vorticity–potential method for three-dimensional duct flow simulations', *Int. j. numer. methods fluids*, **6**, 35–45 (1986).

13. G. J. Hirasaki and J. D. Hellums, 'Boundary conditions on the vector and scalar potentials in viscous three-dimensional hydrodynamics', *Q. Appl. Math.*, **28**, 293–296 (1970).
14. H. Yang, 'Three-dimensional calculation of internal flow using vorticity–potential method', *Ph.D. Thesis*, Ecole Polytechnique de Montreal, 1988.
15. G. D. Raithby, 'Skew upwind differencing scheme for problems involving fluid flow', *Comput. Methods Appl. Mech. Eng.*, **9**, 153–164 (1976).
16. R. J. Goldstein and D. K. Kreid, 'Measurement of laminar flow development in a square duct using a laser–Doppler flowmeter', *ASME J. Appl. Mech.*, **38**, 813–818 (1967).
17. L. S. Han, 'Hydrodynamic entrance lengths for incompressible laminar flow in rectangular ducts', *J. Appl. Mech.*, **27**, 403–409 (1960).
18. Y. Mori, Y. Uchida and T. Ukon, 'Forced convective heat transfer in a curved channel with a square cross section', *Int. J. Heat Mass Transfer*, **14**, 1787 (1971).
19. A. D. Gosman and W. M. Pun, 'Calculation of recirculation flows', *Imperial College, Mechanical Engineering Department Report*, 1973.